Chapter 7
Experimental Comparison of Feedback Control Methods for Active Vibration Damping with Piezoelectric Sensor/Actuator Pairs

Amirali Sadeqi, Jan Høgsberg, Niels L. Pedersen, and Ayech Benjeddou

Abstract This paper presents a comparison of the most common feedback control methods for collocated piezoelectric transducers, including integral force feedback (IFF), direct velocity feedback (DVF), proportional-derivative feedback (PDF), and positive position feedback (PPF). The methods are assessed experimentally with a laboratory setup comprising a set of piezoelectric transducers mounted symmetrically on a cantilever beam as collocated sensor/actuator pairs. The control laws are developed based on voltage-based expressions to be directly tuned and implemented in the experiments with low-cost real-time control boards. The active damping of the feedback control methods is quantified, and the comparison between them underlines the superiority of the presented PPF control in attainable damping. The findings from the experiments can be used to suggest rules of thumb for digital implementation and tuning of collocated feedback controls using piezoelectric sensor/actuator pairs.

Keywords Active vibration damping · feedback control · piezoelectric transducers · collocated sensor/actuator · IFF · DVF · PPF · PDF

Introduction

Passive vibration control systems are simple regarding integration and operation but provide small forces and may not achieve desired damping targets in all applications. For instance, viscoelastic materials are appropriate for high frequencies, the performance of shunt damping depends on the electromechanical coupling, and the dielectric elastomers require high voltages and provide a high impedance and low actuation [1–5]. On the other hand, active vibration control systems allow for damping optimization according to the system's dynamic properties and modal characteristics. One of the common approaches is collocated active control, which requires the sensor and actuator to be mounted at the same point in the structure. Such a pair can provide strong damping by relating their input/output through a control law such as positive position feedback (PPF), proportional-derivative feedback (PDF), integral force feedback (IFF), and direct velocity feedback (DVF). Regarding the two latter, the phase difference between the local force feedback due to the integral or derivative of the sensor measurements provides an unconditionally stable and decentralized control system. It has been demonstrated that the IFF, DVF, and PPF can be robust and significantly reduce vibration amplitudes if the control parameters are tuned and optimized [1, 2, 6–8]. Meanwhile, studies have reported the use of proportional-derivative control in nonlinear applications such as vibration suppression of rotating blades and micro-contact systems [9–11].

Piezoelectric materials have simultaneous actuation and sensing abilities and have been extensively used for active control and vibration damping. They are typically low-cost and lightweight with low power consumption, but require high voltages to generate significant forces and deformations in order to effectively contribute to control, especially for massive structures. They also have the flexibility to be customized in various sizes and shapes for energy harvesting, vibration

Amirali Sadeqi · Jan Høgsberg · Niels L. Pedersen
Department of Civil and Mechanical Engineering, Technical University of Denmark, Denmark
e-mail: amisa@dtu.dk; jahog@dtu.dk; nlpe@dtu.dk

Ayech Benjeddou
Roberval (Mechanics, Energy and Electricity), Université de technologie de Compiègne, Compiègne, France; Institut Supérieur de Mécanique de Paris, Saint Ouen, France
e-mail: ayech.benjeddou@isae-supmeca.fr

Matthew Whelan et al. (eds.), *Dynamics of Civil Structures, Vol. 2*, Conference Proceedings
of the Society for Experimental Mechanics Series, https://doi.org/10.13052/97887-438-0147-4_7

absorbers, and biomechanical applications [4, 12]. It has been suggested that an active element consisting of a collocated piezoelectric actuator-sensor can behave like a muscle [1, 13]. So, as applied to a space truss, one can substitute some structural elements with the active elements to achieve a large enough extension to control the structure.

The IFF damping and performance were compared later with passive resistive and inductive shunting by adding the electromechanical coupling factor as the second control index,[14]. Apart from the drawbacks in the modal fraction index to quantity damping, IFF was reported to be more effective in achieving critical damping compared to classical DVF. In contrast, DVF is more efficient if the piezoelectric transducers have a small mechanical impedance and are softer and smaller than the structure [2]. The PD controller, in general, adds the derivative of the process error to the proportional control output. However, PD feedback (PDF) with a collocated sensor-actuator can be considered an extension of DVF. The simplicity, guaranteed stability, compatibility with physics-based models, and susceptibility to improvement have made both IFF and DVF appealing control laws for various applications. Yet, they have some limitations, such as low damping for high-order modes and practical instability (or loss of compliance at low frequency) due to high-pass filtering of the control signal [15].

On the other hand, PPF, compared to IFF and DVF, is more sensitive to the sampling frequency and tuning control parameters to remain stable. However, it can achieve higher damping in real-time campaigns and be easily implemented in analog circuits to suppress multiple vibration modes, given that they are known beforehand. One can apply optimization methods such as genetic algorithms to achieve multiple control gains [16]. Fractional-order exponents have also been applied as an alternative to tuning PPF control parameters with integer exponents. The studies have demonstrated the efficiency of fractional-order PPF for requiring less actuation voltage [17] and higher robustness in a broader band of effective phase compensation [18]. Yet, the effectiveness, efficacy, and suitability of IFF, DVF, and PPF, as well as their extensions and modified versions, may vary from one case to another.

The underlying project supporting the present work, seeks the possibility of a control system to suppress forearm tremors, which are rhythmic involuntary muscle contractions with noticeable shaking in the upper limb. Various pharmacological and non-pharmacological treatments have been introduced to overcome tremors and ease the patients' posture at rest or action [19]. Non-pharmacological and non-invasive aids, such as robotic assists and wearable orthoses, are commonly used for tremor suppression. Patients must carry such instruments all the time, which can restrict or discomfort the movement [20]. This work investigates the primary challenges of designing and implementing a semi-invasive active control system attached to the forearm bones. To that end, in the following, a cantilever beam with a piezoelectric sensor-actuator pair is experimentally studied. The voltage-based electro-mechanical equations of the classic control methods, IFF, DVF, PDF, and PPF, are derived, and their performance is assessed and compared.

Feedback Control by Sensor/Actuator Pairs

Figure 1 illustrates the schematic of the vibration control system to be investigated here. It comprises a cantilever beam with a collocated piezoelectric sensor/actuator pair. The beam is excited by the external force in the transverse y-direction, while the control by the piezoelectric pair introduces opposite bending moments at the two points of attachment (i and j).

Considering only the axial contribution of the piezoelectric transducers, the sensor deformation Δu_s and actuation force f_a can be related to the measured sensor voltage V_s and the prescribed actuation voltage V_a, respectively, through the electromechanical coupling parameter θ, and the blocked capacitance in constant strain C_p, by the two expressions [13, 21]:

$$\Delta u_s = -\frac{C_p}{\theta} V_s \tag{1}$$

$$f_a = \theta V_a \tag{2}$$

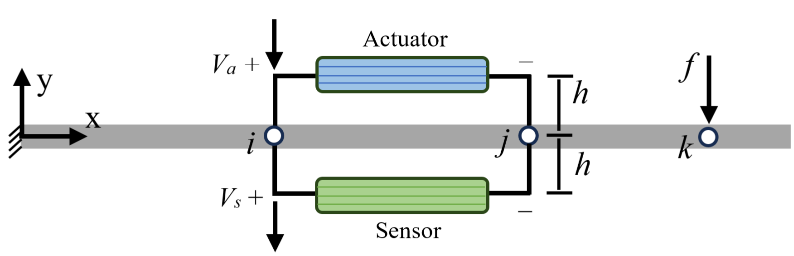

Fig. 1 Schematic of a cantilever beam with a collocated piezoelectric actuator/sensor pair. The offset of each piezoelectric transducer is h to the beam's neutral axis.

Here, θ is obtained as $\theta = d_{31} A_p E_p / t_p$ where A_p, t_p, E_p, and d_{31} are the piezoelectric transducer's area of cross-section, thickness, elastic modulus, and strain coefficient, respectively. Also, by ignoring the transducer's inertia and damping, the relation between the sensor's force and deformation becomes:

$$f_s = -k_s \Delta u_s \tag{3}$$

where k_s is the stiffness of the piezoelectric sensor, which is assumed to be identical to the stiffness of the corresponding piezoelectric actuator, i.e. $k_s = k_a$.

Integral force feedback (IFF)

When using a force sensor to measure the sensor force f_s, inspired by the classical integral force feedback method from [13], the desired actuation force f_a is prescribed by the present IFF control via the direct integral relation:

$$f_a = g' \int f_s dt \tag{4}$$

in which g' is the control gain that scales the required control force for the actuator relative to the measured force from the sensor. In the present application, the above force relation must be converted to a voltage-based control law. By substituting Δu_s from Eq. (1) into Eq. (3), followed by substitution of f_s from Eq. (3) and f_a from Eq. (2), the force-relation in Eq. (4) can be expressed in the desired voltage-form as:

$$V_a = g \int V_s dt \tag{5}$$

defining the normalized gain $g = g' k_s C_p / \theta^2$ for this voltage-based IFF, where the sensor voltage is integrated in real time to determine the actuator voltage upon scaling with the gain g. Hence, instead of a force sensor, one can directly use a piezoelectric voltage and Eq. (5), which provides maximum damping if g is tuned to be optimal in experimental testing. It is noteworthy that depending on the wiring conditions of the sensor and actuator, the current directions change, and g might have a positive or negative sign. According to Fig. 1, the sensor and actuator in this experiment have the same wiring direction, whereby $g > 0$.

Direct velocity feedback (DVF)

The desired actuation force in the DVF control sense can be related to the axial velocity $\Delta \dot{u}_s$ as:

$$f_a = -g' \Delta \dot{u}_s \tag{6}$$

where g' is the control gain when using a velocity sensor. Substituting f_a from Eq. (2) and the derivative of Δu_s from Eq. (1) into Eq. (6), and defining $g = g' C_p / \theta^2$, the required voltage to reach a desired actuator velocity based on DVF follows from:

$$V_a = g \dot{V}_s \tag{7}$$

Hence, when measuring the transducer's voltage rate $\dot{V}_s$ instead of the velocity $\Delta \dot{u}_s$ in (6), the control gain, $g > 0$, is the single parameter to be tuned optimally to achieve maximum damping.

Proportional-derivative feedback (PDF)

Including inertial and stiffness terms in Eq. (6), one can extend the actuation force into the general control law:

$$f_a = -g_1' \Delta \ddot{u}_s - g_2' \Delta \dot{u}_s - g_3' \Delta u_s \tag{8}$$

Similar to Eq. (7), a voltage-based equation can be obtained by eliminating Δu_s and f_a from Eqs. (1) and (2), respectively. To simplify the otherwise general control equation (8), the apparent inertia term is cancelled by $g_1' = 0$. Hereby, the desired proportional-derivative feedback (PDF) control is obtained as:

$$V_a = g_1 \dot{V}_s + g_2 V_s \tag{9}$$

where $g_1 > 0$ is the derivative gain and $g_2 > 0$ is the proportional gain to be tuned to the optimal values, resulting in maximum damping.

Positivie position feedback (PPF)

The PPF control, in general, applies a second-order low-pass filter, in the following referred to as 2^{nd}-order PPF. Disregarding the actuator's inertia, the simpler 1^{st}-order PPF can also be efficiently applied to feedback control using a collocated actuator/sensor. The voltage-based control equations for both are developed in the following.

2^{nd}*-order PPF*

The governing equation of motion of the actuator can be expressed in terms of the displacement δ, damping ratio ζ_a and angular cut-off frequency ω_a [22, 23]:

$$\ddot{\delta} + 2\zeta_a\omega_a\dot{\delta} + \omega_a^2\delta = \omega_a^2\Delta u_s \tag{10}$$

where the actuation force and displacement can be scaled with a gain g' as $f_a = -g'\delta$.

Substituting Δu_s from Eq. (1) and $\delta = -f_a/g'$ into Eq. (10), also eliminating f_a using Eq. (2), the PPF control can be re-written into the desired voltage-based format as:

$$\ddot{V}_a + 2\zeta_a\omega_a\dot{V}_a + \omega_a^2 V_a = g\omega_a^2 V_s \tag{11}$$

where $g = g'C_p/\theta^2$ is the control gain. This PPF control achieves maximum damping, once the control parameters ω_a, ζ_a and g are optimally tuned. It is noteworthy that one may find Eq. (10) in the literature, e.g., [8, 17, 18] stated in terms of modal coordinates.

1^{st}*-order PPF*

Deriving optimal tuning relations for the above 2^{nd}-order PPF may follow various objectives, i.e., maximising damping or minimising vibrations by a resonant control. Thus, reducing the second-order format to a simpler first-order control may be convenient and ease in tuning. In Eq. (11), the apparent inertia term can be cancelled by letting $\omega_a \to \infty$. Hereby, the simpler first-order PPF control can be expressed as:

$$\dot{V}_a + \frac{1}{\tau}V_a = \frac{g}{\tau}V_s \tag{12}$$

when introducing the time-scale $\tau = 2\zeta_a/\omega_a$ and the non-dimensional control gain $g = g'C_p/\theta^2$. In this 1^{st}-order PPF, the apparent gain $g > 0$ and time-scale $\tau > 0$ must be tuned to maximum damping during the experiments.

It is noted that for the present PPF control, a vanishing control effort can be achieved by either $g = 0$ or $\tau \to \infty$. As argued in the following section, the desired complex pole properties in root-locus diagrams are obtained by choosing the time-scale τ as the variable control parameter, whereby the short-circuit limit is recovered when $\tau \to \infty$.

The implementation of equations introduced for IFF and DVF is straightforward, as the actuation voltage V_a can be obtained using the direct integral or derivative of the sensor's voltage measurements V_s. Meanwhile, obtaining the actuation voltage from the ordinary differential equations (11) or (12) is more time-consuming as it requires a numerical integration scheme such as the Euler method [24]. However, as demonstrated later in the experimental analysis, the PPF control outperforms the direct methods, due to its ability to apply a negative stiffness component [25].

Optimal Tuning and Maximum Damping

For the piezoelectric feedback control strategies outlined in the previous section, the theoretical tuning of the control parameters relies on maximizing the modal damping ratio for the targeted vibration mode, which, in the present case, is the fundamental first bending mode of the cantilever.

For all feedback control strategies, the governing closed-loop poles will follow semi-circular trajectories in the complex frequency plane for an increasing damper parameter. An example is illustrated in Fig. 4 for the 1^{st}-order PPF control in Eq. (12). The semi-circular path is for this 1^{st}-order PPF obtained by varying the time-scale τ for a fixed control coefficient g, with $\omega = \omega_0$ representing the natural frequency of the closed-loop system when $\tau \ll 1/\omega_1$, while the opposite limit $\omega = \omega_\infty$ is reached when $\tau \gg 1/\omega_1$. It follows directly from Eq. (12) that $V_a = 0$ when $\tau \to \infty$, whereby ω_∞ corresponds to the natural frequency of the cantilever when the actuator piezo is short-circuited.

It follows directly from the construction of the semi-circular root-locus trajectory in Fig. 4, that the damping ratio associated with the top of the half-circle is approximately

$$\zeta_{max} = \frac{\mathrm{Im}[\omega]}{|\omega|} \simeq \frac{\frac{1}{2}(\omega_\infty - \omega_0)}{\frac{1}{2}(\omega_\infty + \omega_0)} = \frac{\omega_\infty - \omega_0}{\omega_\infty + \omega_0} \tag{13}$$

where $\omega_{opt} = \frac{1}{2}(\omega_\infty + \omega_0) \simeq |\omega|$ approximates the argument of the complex natural frequency.

The present section presents a so-called Modal Control Coupling Factor (MCCF) and expressions for the optimal tuning of the simplest control methods introduced in the previous section. The concept behind the MCCF and the tuning methods has been presented recently in [26], while further details will be derived in [27].

DVF and IFF

For the DVF control in Eq. (7), when $g = 0$, the actuation voltage $V_a = 0$ and the control force $f_a = \theta V_a$ vanishes as well, whereby the short-circuit condition is retained. In the opposite limit $g \to \infty$, the closed-loop system – in theory – becomes undamped at a larger natural frequency $\omega_\infty > \omega_0$. In practice, this limit might be difficult to reach, as the actuator voltage V_a in Eq. (7) scales directly with g. Instead, the limiting frequency ω_∞ can, for the DVF control, be determined numerically, assuming that the piezoelectric actuator link becomes fully rigid. The tuning of the feedback control depends on the properties of the piezoelectric actuator, via the apparent electric stiffness θ^2/C_p, the modal properties of the structure and a modal control coupling factor (MCCF), defined as

$$K_1^2 = \frac{\omega_\infty^2 - \omega_0^2}{\omega_0^2} \tag{14}$$

where subscript 1 denotes the fundamental mode as the control target. The optimal gain scales directly with the MCCF in the following way [27],

$$g_{opt} = K_1^2 \frac{C_p k_1}{\theta^2 \omega_1} \tag{15}$$

where k_1 is the modal stiffness for the mode shape normalized to unit deflection across the actuator terminals.

For the IFF control, the only change relative to DVF is the phase delay of the control, whereby the optimal gain g in Eq. (5) will scale inversely with the natural frequency. Thus, for IFF, the optimal control will be

$$g_{opt} = K_1^2 \frac{C_p k_1 \omega_1}{\theta^2} \tag{16}$$

It is worth noting that the optimal gain g for both DVF and IFF scale with the MCCF K_1^2 and with the modal stiffness k_1, while it is inversely proportional to the electric stiffness θ^2/C_p of the piezoelectric transducer. For the DVF control, the natural frequency ω_1 in the denominator of (15) accounts for the time-differentiation in (7). Thus, for the IFF control gain in (16), ω_1 must appear oppositely in the numerator because of the integration performed in the control equation (5). The present results show that while the attainable damping ratio in Eq. (13) is evaluated directly by the limiting natural frequencies, the optimal tuning expressions require knowledge of both piezoelectric and modal system parameters.

1^{st}*-order PPF*

For the 1^{st}-order PPF control in Eq. (12), either the timescale τ or the gain g can be chosen as the tuning variable. However, to obtain the desired semi-circular root locus trajectory in Fig. 4, the timescale τ must be used as the control variable, while g is chosen within the stability limit associated with PPF control.

As mentioned previously, the fundamental short-circuit limit is retained by $\omega = \omega_\infty$ when $\tau \to \infty$. In the opposite limit ($\tau \to 0$) it follows from Eq. (12) that $V_a \to gV_s$, is experienced by the cantilever beam as a negative stiffness that reduces the natural frequency, i.e. $\omega_0 < \omega_\infty$.

For the 1^{st}-order PPF, the MCCF is formally defined as for the DVF in Eq. (14). However, because ω_∞ corresponds to the short-circuit natural frequency of the beam, the MCCF is conveniently defined relative to this short-circuit frequency as:

$$K_1^2 = \frac{\omega_\infty^2 - \omega_0^2}{\omega_\infty^2} \tag{17}$$

The difference between the two definitions in Eq. (14) and Eq. (17) is small for typical levels of control authority. The optimal tuning of the control timescale can then be approximated as (see [27]):

$$\tau_{opt}\omega_1 = \frac{g}{K_1^2}\frac{\theta^2}{C_p k_1} \tag{18}$$

For very large timescales τ, the 1^{st}-order PPF must recover the IFF in Eq. (5) with g in IFF being equal to g/τ for the 1^{st}-order PPF. This equivalence is verified by comparison of the two tuning formulae in Eq. (16) and Eq. (18), respectively.

Tuning in practice

It is seen from the three tuning expressions in Eq. (15) for DVF, in Eq. (16) for IFF and in Eq. (18) for the 1st-order PPF control, that the tuning scales with the MCCF K_1^2, while it also depends on the modal properties, in the present case the modal stiffness k_1 and natural frequency ω_1, and the electric stiffening parameter θ^2/C_p. Thus, the tuning will most likely require a dedicated numerical model (twin), from which these modal parameters can be derived. As this is beyond the scope of the present analysis, further studies are needed on how to conduct a robust and accurate optimal tuning of collocated feedback control methods for piezoelectric vibration damping.

The above expressions for optimal tuning clearly show that the MCCF (K_1^2) is a crucial governing parameter, which may be determined experimentally by either Eq. (14) or Eq. (17), if the two limiting frequencies ω_0 and ω_∞ can be determined. For IFF in Eq. (5) and DVF in Eq. (7), the issue is associated with the determination of ω_∞, which requires the gain to be very large. For the filtered control in 1^{st}-order PPF, large control efforts are instead associated with the timescale $\tau \to 0$ (which gives ω_0).

In the following experimental campaign, the optimal control parameters for the various control methods are determined by ad-hoc parameter variation for a sinusoidal loading of the cantilever. To determine the associated optimal natural frequency, impact tests are then performed to derive ω_{opt}. As illustrated in Fig. 4, the optimal frequency can be assumed to represent the mean value of the two limiting frequencies: $\omega_{opt} = \frac{1}{2}(\omega_0 + \omega_\infty)$. In the following, either ω_0 (for IFF and DVF) or ω_∞ (for 1st-order PPF) can be determined as the short-circuit frequency, while the other limiting frequencies can be eliminated in the expressions for K_1^2 by the estimated ω_{opt}. The determined MCCF K_1^2 can then be used to determine the damping ratio in (13), which may be re-formulated as

$$\zeta_{max} \simeq \frac{\omega_\infty - \omega_0}{\omega_\infty + \omega_0} = \frac{\omega_\infty^2 - \omega_0^2}{(\omega_\infty + \omega_0)^2} \simeq \tfrac{1}{4}K_1^2 \tag{19}$$

when introducing $\omega_\infty + \omega_0 \simeq 2\omega_0$ or $2\omega_\infty$. This estimated optimal damping ratio can then be compared with the decay rates obtained during impact tests. The latter expression for the damping ratio in (19) is identical to that derived in [28] for piezoelectric vibration damping using a pure resistive shunt.

For the control methods not explicitly tuned in the present section, the calibration procedures are too extensive for the present analysis or have several (sometimes detrimental) objectives. Thus, these are not addressed directly, and only tuned manually by the ad-hoc calibration applied in the following experimental section.

Experimental Setup

The objective of the present experimental analysis is to examine the feedback control methods introduced in the previous section through the experimental vibration of a cantilever beam. Figure 2 exhibits a photo of the setup and instruments from the top and front views. It consisted of an aluminium cantilever beam ($300 \times 30 \times 1.6$ mm) with two collocated piezoelectric pairs, i.e., four patches ($40 \times 13 \times 0.5$ mm). The four piezoelectric patches are identical and made of Lead Zirconate Titanate (PZT) 5A4E piezoceramic material (Piezo Systems, Inc) with the strain piezoelectric coupling constant, $d_{31} = -190 \times 10^{-12}$ m/V and other characteristics presented in Table 1.

Table 1 Characteristics of the applied transducers, D220-A4-303XE, 5A4E PZT, Piezo Systems, Inc.

Weight (gr)	Stiffness (N/m)	Capacitance (nF)	Rated voltage (V)	Resonant frequency (kHz)	Free deflection (μm)	Blocked force (N)
2.7	7×10^6	52	±90	24.5	±3.6	±26

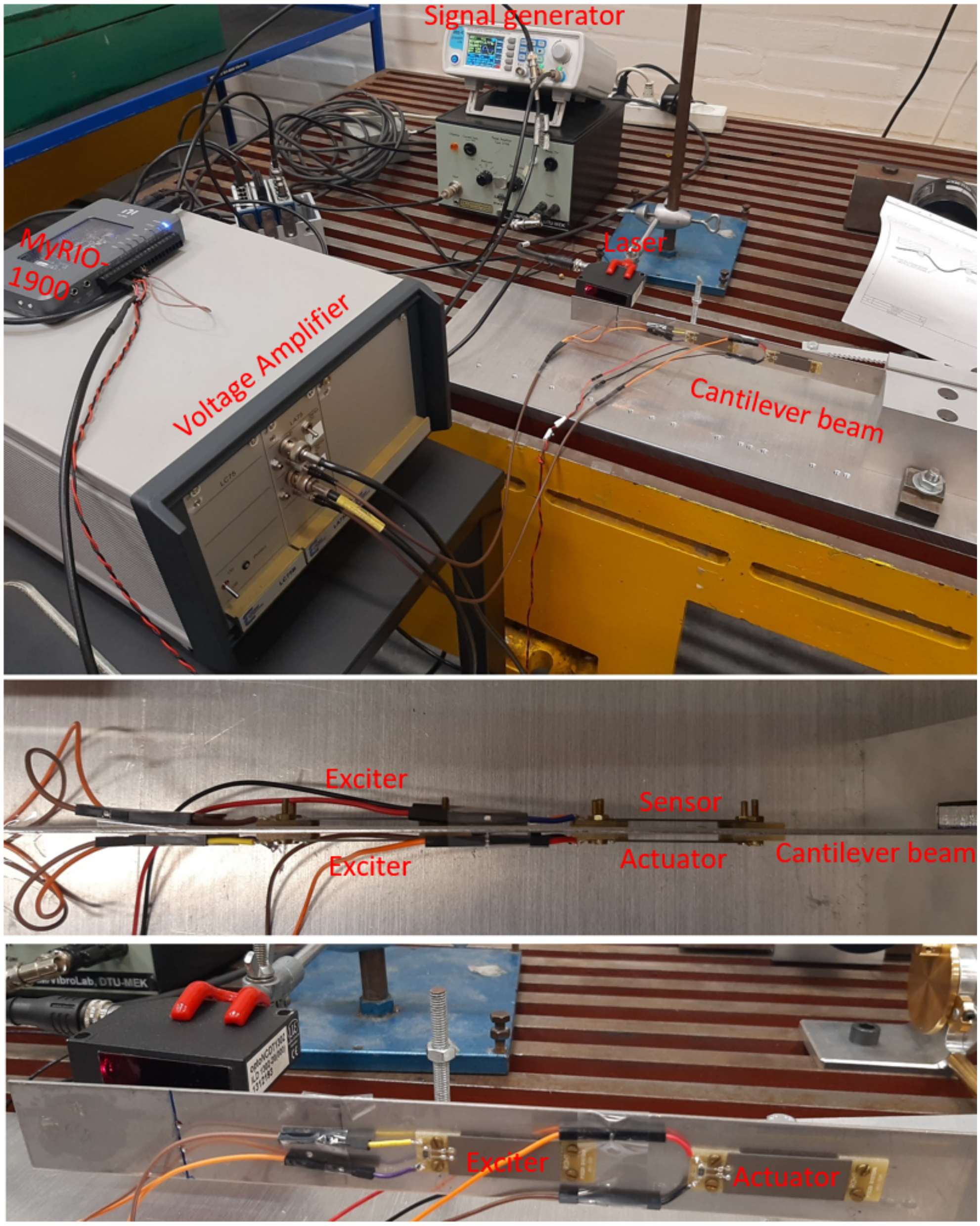

Fig. 2 Experimental test setup of a cantilever beam with piezoelectric patches and data logging system.

The patches were connected to the beam with a gap distance of $h = 2$ mm. The first pair of patches close to the free end (125 mm from the tip) was used to excite the beam. The next two patches close to the support (50 mm from the support) were used as a sensor/actuator pair. The data logging system consisted of a portable device, National Instruments MyRIO 1900, to process the input/output (sensor/actuator) signals in Lab VIEW installed on a computer, InteCorei7-3.8GHz-RAM16GB. A laser sensor (Micro-Epsilon, otpoNCDT-1302) also measured the displacement at the free end of the beam only to monitor the performance of the control, i.e. its measurements were not used in the control loop.

Two types of experiments were perfomred based on impact and resonance excitations. First, the system's frequencies and damping ratios are identified when the (PPF) control is off and on and the beam is subjected to impacts. In that case the exciter piezoelectric pair was short-circuited and they had only elastic contributions. In order to sustain the vibration and increase the signal-to-noise ratio when the control is turned on and causing significant damping, multiple impacts via a small hammer were applied around the free end of the beam.

In the second experiment, the performance of the control methods is assessed when the structure is excited by a sine wave with the first resonance frequency of 13.8 Hz. The sine wave was generated via a signal generator and applied to the first piezoelectric pair, see Figure 2, with the ± 90 V range realized through an intermediate voltage amplifier. Next, the sensor measures the vibration-induced voltage V_s and sends it as a feedback input to MyRIO 1900 and the control environment developed in Lab VIEW. Applying IFF, DVF, PDF, or PPF to the input voltage signal yields the prescribed output voltage signal to be sent from MyRIO1900 to the voltage amplifier and then to the actuator. The tests were performed in equal conditions and a time step of 10^{-4} s for all the control methods in 60 s, while the control was off in the first 30 s.

Modal identification via impact test

The displacement of the beam subjected to multiple impacts was measured via the laser sensor at the free end. Figure 3 shows the displacement time history and power spectral density (PSD) when no control is applied. Employing the displacement time history data in a stochastic subspace identification (SSI) algorithm yields the frequencies 13.80 Hz and 83.79 Hz and the damping ratios 0.61% and 1.06% for the first two vibration modes, presented in Table 2.

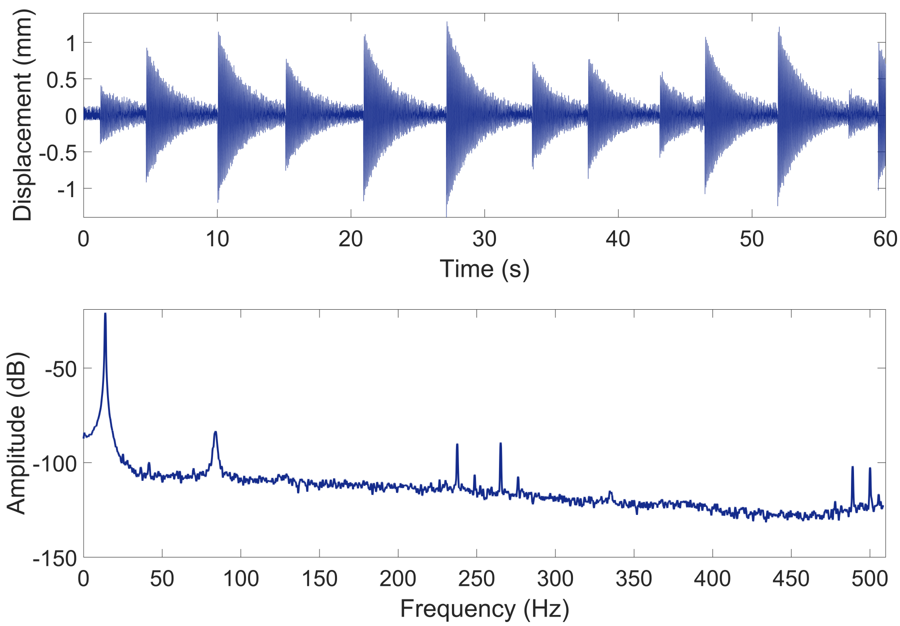

Fig. 3 Displacement time history (top) and PSD (bottom) when the control is off and the beam is subjected to multiple impacts

When applying the control, for example the 1^{st}-order PPF, the poles of the closed-loop system for a given gain g vary with τ, as shown in Figure 4. Hence, for the given g, there is an optimal τ that results in the maximum imaginary part of the eigenvalue.

So, the optimal damping ratio, ζ_{opt}, and the MCCF, K_1^2, can be obtained from Eqs. (13) and (17), respectively. In practice, ω_{opt} is achieved by searching for the optimal τ in a finite range. Also, ω_∞ can be achieved by setting τ to a large value. Meanwhile, ω_0 is difficult to reach in practice as setting τ to zero can prescribe infinite voltage to the actuator beyond its operational range. However, from the circular trajectory in Figure 4 one can deduce $\omega_\infty - \omega_{opt} = \omega_{opt} - \omega_0$, and rewrite

Table 2 System's frequencies and damping ratios for the first two modes with and without PPF control

	No Control	$\tau = 100(\text{ s}) \approx$ Infinite	$\tau = 10^{-3}(\text{ s}) \approx$ Optimal	$\tau = 10^{-4}(\text{ s})$
$\omega_1/2\pi(\text{ Hz})$	13.80	13.78	13.22	13.25
$\zeta_1(\%)$	0.61	0.58	3.16	0.81
$\omega_2/2\pi(\text{ Hz})$	83.79	83.77	83.40	83.40
$\zeta_2(\%)$	1.06	1.75	0.44	2.01

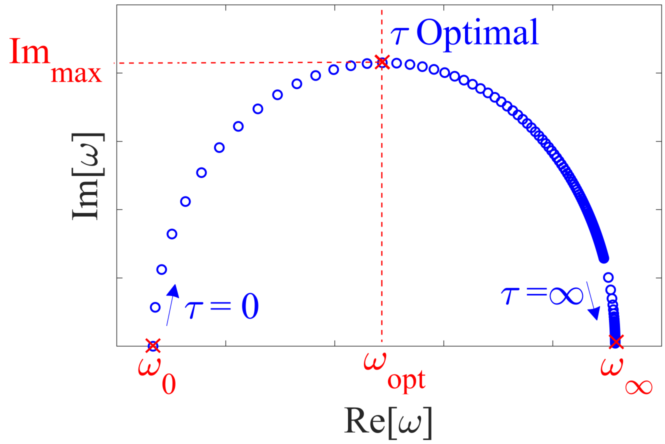

Fig. 4 Real part vs imaginary part of the closed-loop state-space system's eigenvalues (ω) for various τ

Eq. (13) as

$$\zeta_{opt} = \frac{\omega_\infty}{\omega_{opt}} - 1 \tag{20}$$

In the second experiment, the system's frequencies and damping raios are identified in three tests when the beam was subjected to multiple impacts, and the 1^{st}-order PPF was applied with the optimal gain of $g = 3.3$: first, $\tau = 100$ s was chosen as infinity, second, $\tau = 10^{-3}$ s which is found to be the optimal value for damping the first mode, and third, $\tau = 10^{-4}$ s which is the smallest value greater than zero leading to a high actuation voltage. Figure 5 displays the time history of displacement of the free end of the beam in each test and the prescribed actuation voltage. It is seen that the magnitude of the voltage changes reversely with τ so that the displacement diagram for $\tau = 100$ is similar to that in Figure 3.

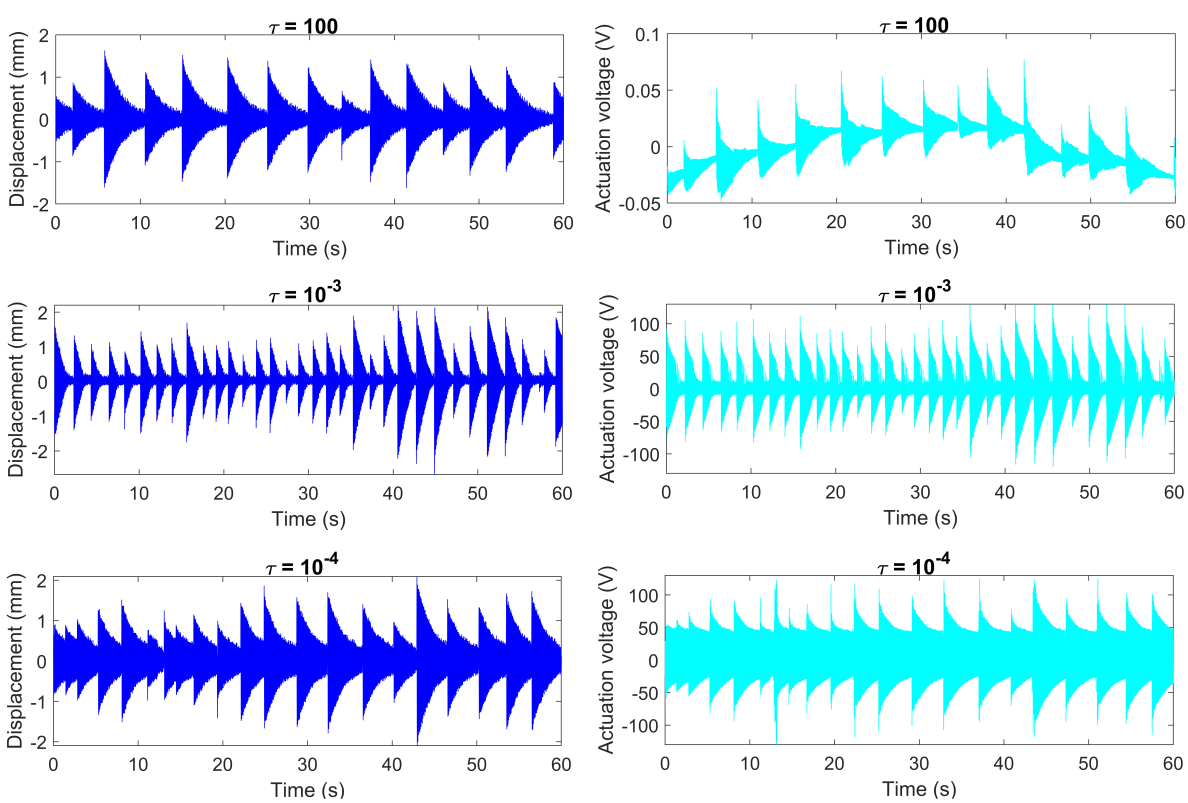

Fig. 5 Displacement and actuation voltage when 1^{st}-order PPF applied and beam subjected to multiple impacts

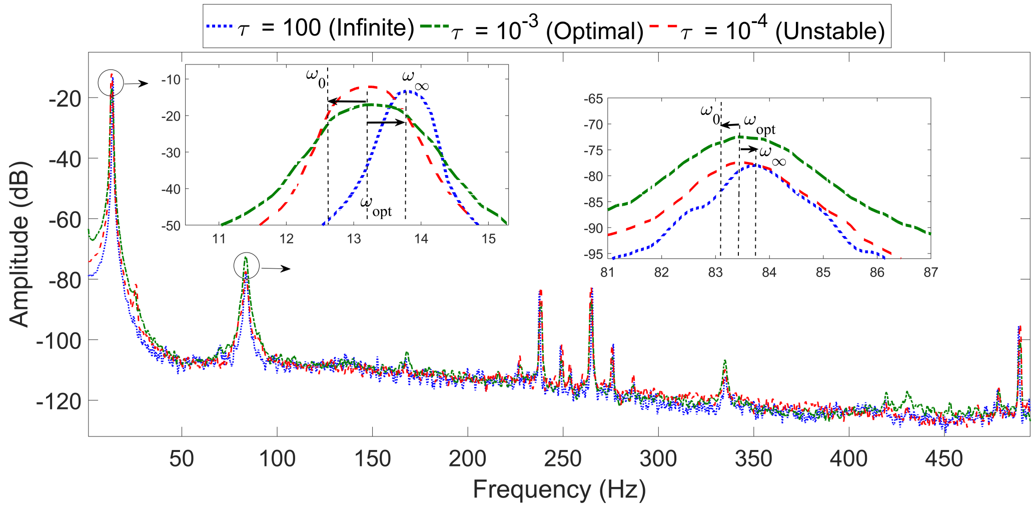

Fig. 6 PSD of the displacement when 1^{st}-order PPF applied and beam subjected to multiple impacts

Figure 6 illustrates the PSD of the displacements. The first two peaks are plotted in the zoomed-insets, and the identified parameters via SSI are tabulated in Table 2. Notably, $\tau = 10^{-4}$ s was the smallest value prescribing actuation voltage in the allowable range. Therefore, there is no actual PSD curve in Figure 6 to represent ω_0 as it corresponds to $\tau = 0$, leading to infinite voltage. However, regarding the circular trajectory in Figure 4, ω_0 is hypothetically demonstrated in Figure 6 to be equidistance with ω_∞ with respect to ω_{opt}.

According to Table 2, the damping ratios (and frequencies) for the case with $\tau = 10^{-3}$ s and 10^{-4} s are almost the same. However, the latter prescribes a higher voltage to the actuator, causing instability and higher amplitude than the optimal case. Furthermore, the optimal damping ratio for the first mode obtained from Eq. (20) is 4.71%, which is about seven times greater than the case with no control (i.e., 0.61%) but different from 3.16% obtained via the identification. The reason is the time-variant nature of the damped response with PPF control in free vibration due to impact. Therefore, the stability of the identified parameters highly depends on the selected state-space model order in SSI. On the other hand, for the second mode, the damping decreases for the optimal τ. Hence, $\tau = 10^{-3}$ s is only valid for the first mode, and every mode requires its optimal gain to achieve maximum damping.

Comparison via resonance test

The performance of the introduced control methods for damping the first resonant mode is assessed herein. The optimal gains presented in Table 3 were applied to Eq. (7) for DVF, Eq. (9) for PDF, Eq. (11) for 2^{nd}-order PPF, and Eq. (12) for 1^{st}-order PPF. The control gain g in the latter was locked to unity since it was found to be less influencing the damping than ω_a and ζ_a. Figures 7 - a to d, show the recorded signals when the IFF control was turned off for 30 s and then was turned on for the next 30 s with an optimal gain. The zoomed-inset figures show the first two seconds after the control activation. Figure 7 - a displays the time history of the applied excitation load (sine wave) via the piezoelectric exciter pair with the resonance frequency of 13.8 Hz. The zero flat lines in Figures 7 - c and d represent the sensor and actuator signals, respectively, when the control is off for 30 s. After activating the control and applying the integral to the sensor's voltage, as introduced in Eq. (5), the optimal gain can be searched for maximum amplitude reduction to prescribe the required actuation voltage. As seen in Figures 7 - c and d, both diagrams drop and become stable in less than 2 s.

Table 3 Optimal gains employed in different control methods

IFF	$g = 2.1 \times 10^{3}$ (1/s)
DVF	$g = 2.2 \times 10^{-4}$ (s)
PDF	$g_1 = 1.8 \times 10^{-4}$ (s), $g_2 = 2$
PPF-1^{st} Order	$g = 3.3,\ \tau = 1.5 \times 10^{-3}$ (s)
PPF-2^{nd} Order	$g = 1,\ \omega_a = 86.5$ (rad/s), $\zeta_a = 0.045$

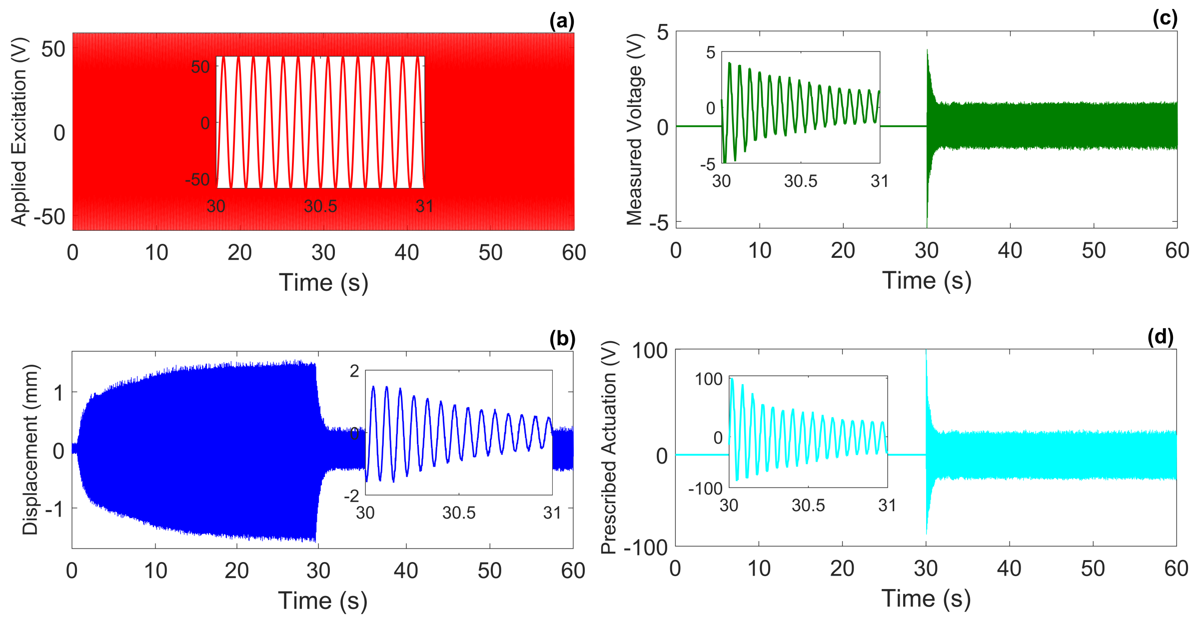

Fig. 7 Time histories of a) applied excitation, b) displacement measured via laser, c) deformation-induced voltage measured via the piezoelectric sensor, d) voltage prescribed to the actuator

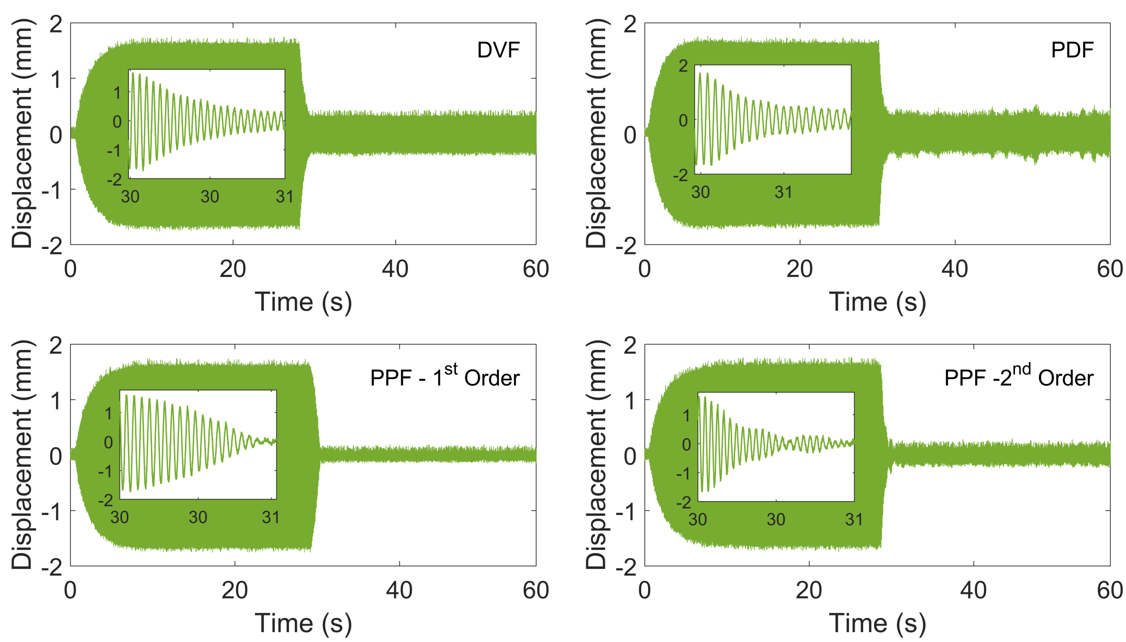

Fig. 8 Displacement time histories measured via laser sensor at the free end of the beam for various controls

A similar trend is observed in Figure 7 - b, representing the displacement of the beam's free end measured via the laser sensor. The vibration amplitude is increasing while the control is off for 30 s. Then, it drops after applying IFF with the optimal gain $g = 2.1 \times 10^3 \mathrm{s}^{-1}$, obtained manually beforehand. Likewise, the next diagrams in Figure 8 exhibit the displacement time histories when applying other controls with optimal parameters. The PPF control demonstrates an overall superior performance compared to IFF and DVF in terms of amplitude reduction. The reduction is quantified and compared through the envelope of displacement settling time presented in Figure 9. Each diagram connects the average of the upper and lower peaks in the displacement time histories in 2.5 s after activating the control (30-32.5 s) but displayed herein from time 0. The 2^{nd}-order PPF and PDF, almost reach 50% amplitude equally fast with a settling time of 0.25 s, slightly faster than DVF and IFF, and about three times faster than 1^{st}-order PPF. However, all controls reach 0.15% of their max amplitude

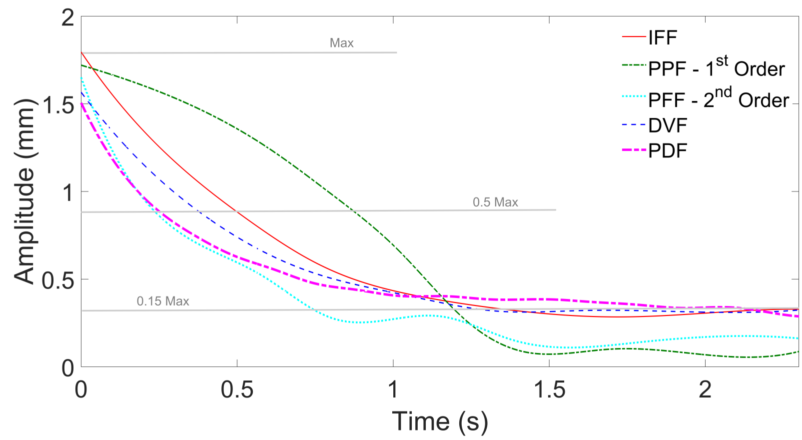

Fig. 9 Envelope of displacement time histories during settling time

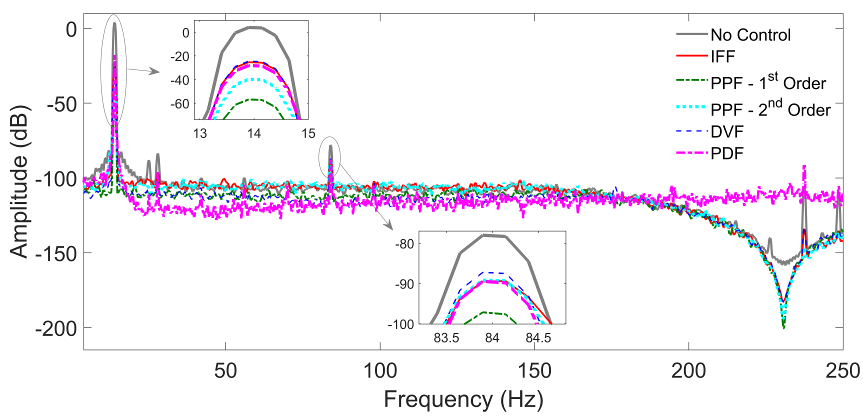

Fig. 10 PSD of displacement and zoomed first two resonant peaks with and without control

almost simultaneously after 1.2 s. The 1^{st}-order PPF provides more significant damping and a lower but more unstable plateau than IFF and DVF, implying an impulse trend of the reduced vibration.

The effectiveness of the controls on the resonance amplitude is also studied in the frequency domain. Figure 10 depicts the PSD of the displacement time histories previously shown in Figure 8. The zoomed insets display the peaks at the first two resonance modes. The grey solid line curve corresponds to the 30 s of displacement when the control is off, whereas the other curves correspond with the next 30 s.

The amplitude of the first mode drops from 4 dB to -24.5 dB with IFF, -25 dB with DVF, and -28 dB with PDF. Meanwhile, the 1^{st}-order and 2^{nd}-order PPF lead to further reduction with -57 dB and -40 dB, respectively. Compared to DVF, the improvement due to having a proportional term in PDF is not remarkable meanwhile subharmonics appear and increase in the latter.

Notably, the actuation voltage for IFF and DVF was obtained using a direct integral and derivative of the vibration-induced voltage measured by the piezoelectric sensor. In contrast, the forward Euler method used for PPF requires further computations than IFF and DVF. In particular, the 2^{nd}-order PPF again requires further computations than the 1^{st}-order PPF, causing a higher plateau in 2^{nd}-order PPF due to data accumulation in the buffer of the processor, whereas it is more efficient at the beginning. Hence, achieving PPF's maximum damping in real-time depends on data logging and signal processing speeds. MyRIO 1900 facilitates input/output processing at a high speed, yet using the FPGA (Field-programmable gate array) feature, one can make the data logging and control process independent from other computations running in parallel in the computer. Despite the excellence of PPF in providing damping in real-time and high-speed processes, the optimal parameters are more complex to find as the control stability can easily be disturbed. Especially when the gain g is not tuned, the control parameters ω_a and ζ_a might be tuned with unrealistic values, such as tuning ζ_a with large values.

Conclusion

This research developed the essential voltage-based relationships for some classic feedback control methods, namely, IFF, DVF, PDF, and PPF, and experimentally assessed their performance. The optimal control gains in IFF, PDF, and DVF were obtained by directly tuning the prescribed actuation voltage. In contrast, the system's resonance frequency was employed in second-order PPF. The superiority of PPF in generating higher damping in the given test setup was found to be considerable compared to IFF, PDF, and DVF, but it is more sensitive to the control parameters and test conditions. Furthermore, the damping generated by PPF depends on data logging and signal processing speeds. It was demonstrated that the second-order PPF leads to a shorter settling time, thus faster vibration reduction. On the other hand, the proportional term in the PDF does not significantly improve its performance compared to DVF. Further investigations regarding the damping mechanism of the discussed control methods in numerical simulations will be conducted in future research.

Acknowledgments The authors would like to acknowledge the Lundbeck Foundation, which has funded this research via the financial support of the project titled "Integrated Tremor Control" (InTreCon) No. 111483.

References

1. Preumont, A., Dufour, J.P., and Malekian, C. "Active damping by a local force feedback with piezoelectric actuators". *Journal of Guidance, Control, and dynamics*, 15(2):390–395 (1992)
2. Monnier, P., Collet, M., and Piranda, J. "Definition of mechanical design parameters to optimize efficiency of integral force feedback". *Structural Control and Health Monitoring*, 12(1):65–89 (2005)
3. Kelley, C.R. and Kauffman, J.L. "Exploring dielectric elastomers as actuators for hand tremor suppression". In *Electroactive Polymer Actuators and Devices (EAPAD) 2017*, volume 10163, pages 368–378. SPIE (2017)
4. Toftekær, J.F. *Resonant Piezoelectric Shunt Damping of Structures*. PhD Dissertation, Technical University of Denmark, (2019)
5. Dietrich, J., Raze, G., Paknejad, A., Deraemaeker, A., Collette, C., and Kerschen, G. "Vibration mitigation of bladed structures using piezoelectric digital vibration absorbers". In *Special Topics in Structural Dynamics & Experimental Techniques, Volume 5: Proceedings of the 40th IMAC, A Conference and Exposition on Structural Dynamics 2022*, pages 91–94. Springer (2022)
6. Zamanian, A.H. and Richer, E. "Adaptive notch filter for pathological tremor suppression using permanent magnet linear motor". *Mechatronics*, 63:102273 (2019)
7. Paknejad, A., Zhao, G., Chesné, S., Deraemaeker, A., and Collette, C. "Design and optimization of a novel resonant control law using force feedback for vibration mitigation". *Structural Control and Health Monitoring*, 29(6):e2939 (2022)
8. Fanson, J.L. *An experimental investigation of vibration suppression in large space structures using positive position feedback*. PhD thesis, California Institute of Technology (1987)
9. Kandil, A. and El-Gohary, H. "Investigating the performance of a time delayed proportional–derivative controller for rotating blade vibrations". *Nonlinear Dynamics*, 91:2631–2649 (2018)
10. Fey, R., Wouters, R., and Nijmeijer, H. "Proportional and derivative control for steady-state vibration mitigation in a piecewise linear beam system". *Nonlinear Dynamics*, 60:535–549 (2010)
11. Hamed, Y.S., Albogamy, K., and Sayed, M. "A proportional derivative (PD) controller for suppression the vibrations of a contact-mode AFM model". *IEEE Access*, 8:214061–214070 (2020)
12. Benjeddou, A., Enriquez, D.J.R., Schicker, J., Binder, A., and Sinani, T. "Experimental characterization of piezoelectric and elastic operational field-dependent non-linearities of multilayer benders for resonant driving of bone-conduction hearing aids via a dual-actuators side-by-side device". *Mechanics of Advanced Materials and Structures*, 31(4):3138–3160 (2024)
13. Preumont, A. *Vibration control of active structures*, volume 179. Springer (2011)
14. Preumont, A., De Marneffe, B., Deraemaeker, A., and Bossens, F. "The damping of a truss structure with a piezoelectric transducer". *Computers & Structures*, 86(3-5):227–239 (2008)
15. Chesné, S., Milhomem, A., and Collette, C. "Enhanced damping of flexible structures using force feedback". *Journal of Guidance, Control, and Dynamics*, 39(7):1654–1658 (2016)
16. Kwak, M.K. and Han, S.B. "Application of genetic algorithms to the determination of multiple positive-position feedback controller gains for smart structures". In *Smart Structures and Materials 1998: Mathematics and Control in Smart Structures*, volume 3323, pages 637–648. SPIE (1998)
17. Marinangeli, L., Alijani, F., and HosseinNia, S.H. "Fractional-order positive position feedback compensator for active vibration control of a smart composite plate". *Journal of Sound and Vibration*, 412:1–16 (2018)
18. Niu, W., Li, B., Xin, T., and Wang, W. "Vibration active control of structure with parameter perturbation using fractional order positive position feedback controller". *Journal of Sound and Vibration*, 430:101–114 (2018)
19. Grimaldi, G. and Manto, M. *Mechanisms and emerging therapies in tremor disorders*. Springer Nature (2023)
20. Nguyen, H.S. and Luu, T.P. "Tremor-suppression orthoses for the upper limb: current developments and future challenges". *Frontiers in Human Neuroscience*, 15:622535 (2021)
21. Preumont, A. *Dynamics of electromechanical and piezoelectric systems*, volume 136. Springer (2006)
22. Goh, C. and Caughey, T. "On the stability problem caused by finite actuator dynamics in the collocated control of large space structures". *International Journal of Control*, 41(3):787–802 (1985)
23. Fanson, J. and Caughey, T. "Positive position feedback control for large space structures". *AIAA journal*, 28(4):717–724 (1990)

24. Butcher, J.C. *Numerical methods for ordinary differential equations*. John Wiley & Sons (2016)
25. Høgsberg, J.R. and Krenk, S. "Linear control strategies for damping of flexible structures". *Journal of Sound and Vibration*, 293(1-2):59–77 (2006)
26. Høgsberg, J., Sadeqi, A., Pedersen, N.L., and Benjeddou, A. "Tuning of positive position feedback for piezoelectric vibration control". In *The 9th International Workshop on Structural Control and Health Monitoring*. International Association on Structural Control and Monitoring (2024)
27. Sadeqi, A., Høgsberg, J., Pedersen, N.L., and Benjeddou, A. "Design and tuning of positive position feedback control by the modal control coupling factor". *In preparation* (2024)
28. Chevallier, G., Ghorbel, S., and Benjeddou, A. "Piezoceramic shunted damping concept: testing, modelling and correlation". *Mechanics & Industry*, 10(5):397–411 (2009)